Linear viscoelastic study of lipid vesicle dispersions: Hard-sphere behavior and bilayer surface dynamics

J. B. A. F. Smeulders, C. Blom, and J. Mellema
Rheology Group, Faculty of Applied Physics, University of Twente, P.O. Box 217, 7500 AE Enschede, The Netherlands
(Received 19 March 1990)

The frequency-dependent complex viscosity of dispersions of various lipid vesicles was measured. Two clearly distinguishable features in these curves could be observed, suggesting two relaxation processes. The first relaxation time is shown to be dependent on the third power of the vesicle radius. This implies an elasticity of entropic nature, which is the result of the translational ordering of the vesicles that are subjected to shear flow and forced out of their equilibrium distribution. A comparison with linear viscoelastic measurements of dispersions of "real" hard-sphere (silica) particles shows remarkable agreement, and trends are extended. Furthermore, the measurements support theoretical work. For the second relaxation process, a linear dependency of the relaxation time on the radius of the vesicle is observed. In addition, the relaxation time and the effective viscosity were found to be linearly proportional. A combination of various similar theories that treat the dynamics of spherical capsules in terms of capsule wall viscoelasticity proved capable of explaining the dependency of the second relaxation time on the product of radius and effective viscosity. The second relaxation process was found to be pertaining to the surface shear viscoelasticity of the vesicle wall. Thus, from the analysis of the data with theory, the surface shear modulus and the surface shear viscosity of the lipid bilayer could be deduced. Furthermore, a small contribution of the curvature modulus was detected in our measurements, for which an estimate could be given. With the aid of literature data for the curvature modulus, the dilatational modulus, and the present value of the surface shear modulus found in this work, Young's modulus and the Poisson ratio of the investigated bilayer could be established.

I. INTRODUCTION

The macroscopic rheological properties of dispersions in a certain flow field are determined by the momentary morphology of the constituents, the momentary texture of the dispersion, and the relevant interactions on the microscopic scale. These rheological properties strongly depend on the ratio of the time scales of observation and the time scales of the microscopic processes that determine the momentary structure. An increased understanding of rheological phenomena benefits from the availability of well-defined model systems and sophisticated measuring methods. Only quite recently has a very good model system of a colloidal (i.e., submicron) hard-sphere system become available (Van Helden *et al.*[1] and Coehen and De Kruif[2]). The linear and nonlinear rheological behavior of this system is now well mapped out experimentally (Van der Werff *et al.*[3] and Van der Werff and De Kruif[4]).

The complexity of a system starting with a colloidal hard-sphere dispersion can be extended in three directions: adding attractive or repulsive interactions or allowing deformability of the particles without accounting for interparticle interactions. Here, deformability is considered. Unfortunately, only at very short time scales do rubberlike colloidal spheres show interesting rheological behavior due to deformability. According to Fröhlich and Sack,[5] relaxation times can then be expected in the order of 1×10^{-11} s for incompressible spheres with Young's modulus of 5×10^{7} N/m^2 [soft polyvinyl chloride (PVC)]. Such short time scales are difficult to investigate with rheological means. In the present paper deformable colloidal spheres composed of a liquid enclosed by one bilayer of lipid molecules are studied. Such particles, called vesicles, are well defined: They can be made monodisperse in sufficiently large quantities. When the dispersion is not flowing or is flowing slowly, the particles behave effectively as spheres and only above a certain rate of flow or, in harmonic experiments, above a certain frequency, will the particles deform significantly. In the following, measurements of the complex viscosity of lipid vesicle dispersions between 70 Hz and 235 kHz will be presented. According to the preceding considerations, two relevant microscopic time scales can be expected. One pertains to the distribution perturbation of the vesicles (as was recently found for real hard spheres[3]) and the other to the deformability of the vesicles. In Sec. II the theoretical and experimental background of these time scales is summarized. The preparation of the vesicles and the measuring methods are described subsequently in Secs. III and IV. Then, in Sec. V, the measurements and the analysis give evidence that the mentioned microscopic processes take place and, in addition, result in microscopic parameters of elastic and viscous nature characterizing the surface of the vesicle. Finally, in Sec. VI, the results are discussed.

II. THEORETICAL AND EXPERIMENTAL BACKGROUND

In complicated fluids, like dispersions, various microscopic processes can take place that counteract flow.

These processes can be characterized with relaxation times ranging from very long to very short. The viscoelastic behavior of complicated fluids depends on the ratio of these times (relaxation times) and the time it takes to carry out an experiment, e.g., the time equal to the inverse of a certain rate of flow $\dot{\gamma}$ or the time ω^{-1} in a harmonic flow experiment with angular frequency ω. When the microscopic times are shorter than the experimental times, the fluid will not be different from the fluid at rest, and, consequently, no change in viscosity below a certain $\dot{\gamma}$ or ω is observed. When, however, the relaxation times are larger than the experimental time scales, the flow will impose a certain structure on the fluid that changes its resistance to flow. Apparently, the viscosity of a complicated fluid as a function of rate of flow or frequency changes when the experimental time is close to the characteristic time of a microscopic process.

The above-noted considerations sketch a general picture of the viscosity as a function of the ratio between the relaxation time and the experimental time. We should stress that we will be dealing with linear experiments, so let us confine our attention to a harmonically oscillating shear flow in the linear regime. In that case a linear relationship exists between the rate of shear and the shear stress. Writing the relationship with complex quantities, the complex viscosity

$$\eta^*(\omega)=\eta'(\omega)-i\eta''(\omega)$$

is defined: $\sigma^*=\eta^*\dot{\gamma}^*$, with $\dot{\gamma}^*=\dot{\gamma}_0\exp(i\omega t)$, the complex rate of shear, and $\sigma^*=\sigma_0\exp(i\omega t+\varphi)$, the complex shear stress. (t is the time, ω the angular frequency, φ a phase angle, and $i^2=-1$.) In the linear regime, the foregoing sketch about time scales does not only hold for the real part η' of η^*, but now also for the imaginary part η'' of η^*. The imaginary part η'' is pertaining to an energy storage process during a cycle. From the theory of passive linear systems (see, e.g., Flügge[6]), it follows that the angular frequency dependency of η' and η'' for N relaxation processes can be written as

$$\eta'(\omega)=\eta'_\infty+\sum_{p=1}^{N}\frac{G_p\tau_p}{1+\omega^2\tau_p^2} \tag{1a}$$

and

$$\eta''(\omega)=\sum_{p=1}^{N}\frac{\omega G_p\tau_p^2}{1+\omega^2\tau_p^2}\ , \tag{1b}$$

respectively, with relaxation time τ_p and relaxation strength G_p representing the pth microscopic process and η'_∞ the viscosity at infinite frequency. A few relaxation mechanisms will be highlighted in Secs. II A and II B.

A. Hard-sphere diffusion relaxation

In a shear experiment the equilibrium distribution of the particles is disturbed, and, consequently, the entropy decreased. Maximization of the entropy is the driving force behind the relaxation of this imposed structure. Thorough treatment of this problem should involve the many-body distribution function. As hydrodynamics on the many-body level is still a formidable problem which has not as yet been solved, we have to resort to theories that use a pair-distribution-function approximation.

The first treatment of this pair approach was given by Batchelor.[7] From the Batchelor theory, an average relaxation time $\tau_t\equiv(\eta'_0-\eta'_\infty)/G'_\infty$ stemming from the relaxation of a change of the pair distribution of hard spheres can be deduced. [η'_0 is the steady-state viscosity (no new structure imposed), η'_∞ is the viscosity at infinite frequency (new structure imposed), and G'_∞ the storage modulus at infinite frequency.] This prediction holds in the limit of infinite dilution. It could be expressed as

$$\tau_t=0.25\frac{a^2}{D_0}\ , \tag{2}$$

where the diffusion coefficient D_0 equals $kT/6\pi\eta_0 a$. Further, τ_t can be called the translational diffusion relaxation time, a is the radius (for capsules like vesicles it is the distance from the center of the sphere to the outer surface of the sphere), k the Boltzmann constant, T the absolute temperature, and η_0 the solvent viscosity.

According to the same source, the diffusion relaxation strength G_t at infinite dilution is given by the equation

$$G_t=3.9\frac{\phi^2 D_0\eta_0}{a^2}\ , \tag{3}$$

where ϕ is the volume fraction of the dispersion, i.e., the ratio of the total volume that the vesicles occupy and the total dispersion volume.

Russel and Gast,[8] in their study into nonequilibrium statistical mechanics of dispersions of hard spheres, following Batchelor, have taken into account pairwise additive hydrodynamics and a volume-fraction-dependent equilibrium structure. Thus, they evaluated the volume fraction dependency of the translational distribution relaxation strength G_t.

Recently, their work was extended by Wagner and Russel.[9] They incorporated many-body thermodynamic interactions. As this last interaction cannot be evaluated exactly, it has to be estimated. A description is needed at the three-particle level and for this, the three-particle distribution is approximated. This can be done in different ways, depending on the criteria according to which a series is ended (closure). Wagner and Russel have chosen a Percus-Yevick-type closure, a closure based on a modified superposition and one in between. It is not clear in which concentration region the theories should be valid.

Careful study (Van der Werff *et al.*[3]) of the experimental linear rheological data of colloidal hard-sphere dispersions between volume fractions $\phi=0.4$ and 0.6 has demonstrated that a consistent description of all complex shear viscosity measurements could be given with

$$\eta^*-\eta'_\infty=G_1\tau_1\sum_{p=1}^{M}\frac{1}{p^2+i\omega\tau_1}\ , \tag{4}$$

with p representing the number of the relaxation time and with M as the maximum number of relaxation times. G_1 and τ_1 are experimental values characterizing the complex viscosity. One notices that Eq. (4) implies that in

Eq. (1), $G_p = G_1$ and $\tau_p = \tau_1/p^2$. If M and ω are large, then

$$\eta^* - \eta'_\infty = 1.11 G_1 \tau_1^{1/2} \omega^{-1/2}(1-i) \ . \tag{5}$$

This high-frequency behavior has been observed indeed by Van der Werff *et al.*[3]

The theoretical G_t and τ_t may be compared with the experimental G_1 and τ_1 deduced between $\phi = 0.4$ and 0.6. No single theory that is known can satisfactorily account for G_1 and τ_1 throughout these volume fractions. The scaling with a^3 is, however, confirmed. The fact that the $\omega^{-1/2}$ dependency of $\eta^* - \eta'_\infty$ is not predicted by any theory is noteworthy. In the present study one of the observed relaxation phenomena is attributed to the hard-sphere distribution relaxation. The main justification is that it corroborates the experimental data for τ_1, G_1, and η'_∞ (Van der Werff *et al.*[3]).

B. Deformation relaxation

A vesicle in shear flow will be deformed if its surface is not perfectly rigid. Vesicle deformation requires deformation of the bilayer. Three bilayer deformation processes will be highlighted.

(1) Surface shear: This process involves surface deformation at constant area. The elasticity pertaining to this process is the surface shear modulus μ. The dissipative part of this process pertains to ζ, the surface shear viscosity.

(2) Surface dilatation: This involves area changes without shear. The surface dilatational modulus κ and the surface dilatational viscosity σ pertain to this process.

(3) Bending of the surface, involving the curvature modulus K_c.

In addition, local bending of the surface also brings a possible interfacial tension into play since it influences the local pressure difference across the interface.

In Fig. 1 the processes that involve properties (1), (2), and (3) are illustrated. In order to calculate the linear viscoelastic behavior of deformable droplets, the constitutive equation of the droplet interface has to be defined. For an infinitely thin flat surface the most simple linear relationship between the surface stress tensor P and the surface strain tensor E in a harmonic experiment in Cartesian coordinates is given by

$$\mathsf{P} = [\gamma + (\kappa + i\omega\sigma)\mathrm{tr}(\mathsf{E})]\underline{1} + 2(\mu + i\omega\zeta)\bar{\mathsf{E}} \ , \tag{6}$$

where $\underline{1}$ is the unit tensor. $\bar{\mathsf{E}}$ the deviatoric part of E, and $i^2 = -1$. In curvilinear coordinates for a nonflat surface, the expression is more complex but can be found in textbooks (e.g., Aris,[10] page 232). If the curved surface has finite thickness to first order, κ, σ, μ, and ζ remain approximately the same for not too thick surfaces, while a curvature term has to be included (De Bruijn and Mellema[11]). This latter term is characterized with what is called the curvature modulus K_c in physical chemistry literature (e.g., De Gennes[12] and Helfrich[13]) and flexural rigidity in mechanics literature (e.g., Kléman[14]). The relevant curvature energy E_c is

$$E_c = \tfrac{1}{2} K_c \int\int \left[\frac{1}{R_1} + \frac{1}{R_2} - \frac{2}{R_0} \right]^2 dA \ , \tag{7}$$

with $1/R_1 + 1/R_2$ the sum of the principal curvatures at a point on the surface, $1/R_0$ the spontaneous curvature, and dA a surface element.

It has been demonstrated[15] that small deformations of thin isotropic shells (thickness h is small with respect to the inverse of the local curvature) can be described with deformations of a shell with fixed thickness. Then the shell can be characterized with its Young's modulus E and its two-dimensional Poisson ratio ν $(-1 < \nu < 1)$. Here we assume that this approximation is also valid for an insoluble layer (with the condition that E perpendicular to the surface is equal or larger than E along the surface).

Expressed in E and ν, for a layer of fixed thickness h,

$$\mu = \frac{Eh}{2(1+\nu)} \ , \tag{8a}$$

$$\kappa = \frac{Eh}{2(1-\nu)} \ , \tag{8b}$$

and (e.g., Kléman[14])

$$K_c = \frac{Eh^3}{12(1-\nu^2)} \ . \tag{8c}$$

We see that K_c for an insoluble layer with thickness h is not independent of κ and μ.

The mechanical properties in Eqs. 8(a)–8(c) occur in the theories in which the relaxations of surface deformation are calculated and in which hydrodynamics is included (Brunn,[16] Felderhof and Jones,[17] and Van der Linden *et al.*[18]). The implementation of such hydrodynamics into a complete linear viscoelastic theory is more difficult [Oldroyd,[19,20] Barthes-Biesel and Chhim,[21] various papers by Takano and Sakanishi (e.g., Ref. 22) and De Bruijn and Mellema[11]]. To the best of our knowledge, no coupling between surface motions of different droplets

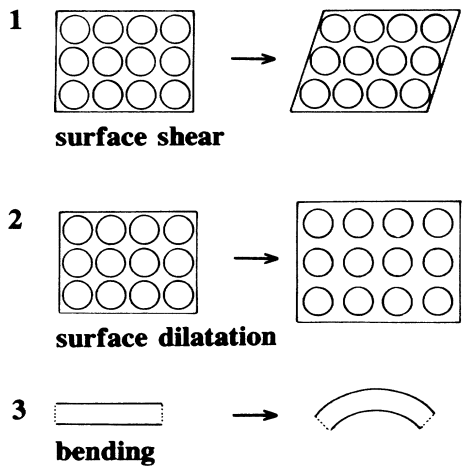

FIG. 1. Some possible deformation processes in the bilayer: (1) and (2), top view; (3), side view. Circles model the section of a lipid molecule.

has been taken into account. To avoid repetitions of general pictures of fluctuating capsules, for which we refer to, e.g., Oldroyd,[19,20] Oosterbroek and Mellema,[23] and De Bruijn and Mellema,[11] we will select some relevant implications and results.

Various investigators (see Table IV) have found that $K_c=(0.4-2.6)\times10^{-19}$J (Refs. 24–30) and $\kappa\simeq0.1$ N/m (Refs. 31 and 32) for egg yolk lipid (EYL) bilayer surfaces (of which our vesicles are composed). The interfacial tension of the EYL bilayer is believed to be very small [$\gamma\ll10^{-3}$ N/m (Refs. 26 and 31)]. For processes pertaining to capsule dynamics we will use as radius the distance from the center of the capsule to the middle of the wall, a_m. So a_m equals $a-\frac{1}{2}h$, where h is the bilayer thickness. The relaxation time τ_κ pertaining to κ is roughly $a_m\eta/\kappa$ (Oldroyd[20] and Felderhof and Jones[17]). For $a_m\simeq100$ nm, $\eta_0\simeq10^{-3}$ Pa s, and $\kappa\simeq10^{-1}$ N/m it follows that $\tau_\kappa\simeq10^{-9}$ s. The complex viscosity η^* can be measured in our laboratory up to 235 kHz. With our apparatus our shortest observable deformation relaxation time is $1/(2\pi\times235\times10^3)\simeq7\times10^{-7}$ s. As we can also learn from the onset of the transition, while not yet actually imposing frequencies corresponding to the relaxation time, in practice we can already measure relaxation times that are about one decade shorter than 7×10^{-7} s, and so are approximately equal to 10^{-7} s. As τ_κ is in the order of 10^{-9} s, this dilatational relaxation process is not observable by us.

The analyses given by Oosterbroek and Mellema,[23] Felderhof and Jones,[17] and De Bruijn and Mellema[11] show that if K_c/a_m^2 is much smaller than κ (K_c/a_m^2 is here 10^{-4} N/m and $\kappa=0.1$ N/m), the observed transition at the lower frequency is determined by γ, μ, and K_c while the not observable one at the higher frequency is determined by κ only. It also follows that $\kappa\gg\mu$, and, consequently, the relevant relaxation time is that at what is called in literature constant surface area. This is only true in first order of deformation of the surface since, obviously, exact area conservation only holds for $\kappa\to\infty$. If the dilatational relaxation process could be observed, the fact that $\kappa\gg\mu$ would mean that the κ transition would be well separated from the lower-frequency deformation transition (pertaining to γ, μ, and K_c).

Surface deformation can be expanded in a series using spherical harmonics Y_{lm} with $m=0,\pm1,\ldots,\pm l$. The deformation with the lowest energy (the largest relaxation time) is the Y_{2m} mode. Combining recent calculations (Felderhof and Jones,[17] Schneider *et al.*,[24] and Milner and Safran[33]) with the pioneering work of Oldroyd,[20] the relaxation time for this mode can be given as

$$\tau=\frac{(23\eta_i+32\eta_0)a_m+16\zeta}{24\{\gamma+\frac{2}{3}\mu+\frac{K_c}{a_m^2}[6-C_0a_m+\frac{1}{2}C_0^2a_m^2]\}} \tag{9}$$

(η_i and η_0 denote the viscosities inside and outside the capsule, respectively, and C_0 is the spontaneous curvature, defined as $-2/a_0$, where a_0 is the natural radius of the bilayer). The intrinsic viscosity $[\eta]$ is defined

$$[\eta]=\lim_{\phi\to0}\frac{\eta-\eta_0}{\eta_0\phi}. \tag{10}$$

For $\omega\ll\tau^{-1}$ it equals

$$[\eta]=\tfrac{5}{2}, \tag{11}$$

and for $\omega\gg\tau^{-1}$, from Oldroyd,[20]

$$[\eta]=\tfrac{5}{2}\frac{23\eta_i-16\eta_0+16\zeta/a_m}{23\eta_i+32\eta_0+16\zeta/a_m}. \tag{12}$$

The effect of this deformation relaxation is hard to detect at low volume fractions. At higher volume concentrations the effect may be observable but (9) is no longer valid. Neither can viscosities any longer be simply expressed as $\eta=\eta_0(1+\phi[\eta])$. If one assumes that the deformation relaxation of an individual droplet is not coupled to that of others except through the influence of their presence in its ambient fluid, (9) can be modified for higher volume fractions by replacing η_0 by the effective viscosity of the dispersion. The effective viscosity is defined as the viscosity at the relevant frequency, so, e.g., $\eta'(1/\tau_{\rm def})$, with $\tau_{\rm def}$ the deformation relaxation time (see also Sec. V B). According to Krieger and Dougherty,[34] the expressions for the viscosities at higher volume fractions valid for $\omega\ll\tau^{-1}$ and $\omega\gg\tau^{-1}$ are related to the intrinsic viscosities (11) and (12). They obtained the following useful equation for the viscosity η of a dispersion of hard spheres:

$$\eta=\eta_0[1-k_p\phi]^{-[\eta]/k_p} \tag{13}$$

and pointed k_p out as the reciprocal of the maximum packing fraction. It can be derived by a mean-field argument, as shown by Ball and Richmond.[35] They pointed out, however, that k_p might be slightly dependent on the volume fraction.

The constant k_p is certainly also dependent on the momentary microscopic structure and, consequently, on the microscopic flow field. To be more precise, deformable spheres behave at low frequencies as hard spheres only if any elastic constant is present in the sphere surface. If, however, the frequency is high enough such that the local microscopic flow field is strong enough to overcome the elastic counterforce in the surface [this implies that in $\eta^*(\omega)$ a deformation transition occurs], then a significant flow field is set up inside the droplet which changes the flow field outside the droplet with respect to hard spheres (Oldroyd[19,20] and Oosterbroek and Mellema[23]). Thus, for deformable droplets at high frequency, k_p need not be equal to the k_p valid for hard spheres.

III. LIPID VESICLES

A. Structure

Vesicles are spherical capsules of which the surface layer is made of biological material. Mostly, the layer consists of various kinds of lipids, sometimes with added cholesterol. The vesicle surfaces have this in common with the walls of various cells in living bodies. A study into the behavior of synthetic lipid membranes is a study into a model system for biological membranes and therefore can contribute to the understanding of the processes that occur in organisms.

The pharmaceutically used word "liposome" applies to spherical capsules of which the wall usually consists of more than one lipid bilayer. To stress the fact that the structures studied here have one bilayer only (are unilamellar), we use the word (lipid) vesicles. Vesicles are dispersed in aqueous environment and contain the same in the inside region. As lipids are strong amphiphiles, they associate in water to minimize their energy: aliphatic tails group together and only the hydrophilic head groups expose to water. The spherical bilayer belongs to the possible configurations. The innermost and outermost regions of this bilayer are polar and in contact with water. The inside consists of the apolar, hydrophobic parts of the lipids and is shielded from water. See Fig. 2(a) for the essentials of the lipid vesicle.

The lipids that form a vesicle can vary greatly in structure and size but among the most commonly used are the phosphatidyl cholines, the structure of which is displayed in Fig. 2(b), where the R groups are long aliphatic chains.

A lipid bilayer of pure lipids in aqueous environment displays a remarkable and sudden change in structure and rigidity at a certain temperature, the transition temperature T_c. Below T_c, the bilayer is a quite rigid structure, in which the lipid tails are rather rigidly aligned. This is called the gel state. Above T_c the bilayer suddenly becomes much more liquid, the lipid tails become more flexible, tails of opposing monolayers interdigitate, and lipids on the whole are more mobile. This condition is called the liquid crystalline state. T_c is very sharply and precisely defined for each lipid assembly, but in the case of a mixture of lipids, there exists a T_c trajectory. In general, T_c is increased by longer hydrocarbon chain lengths and by less unsaturated bonds therein.

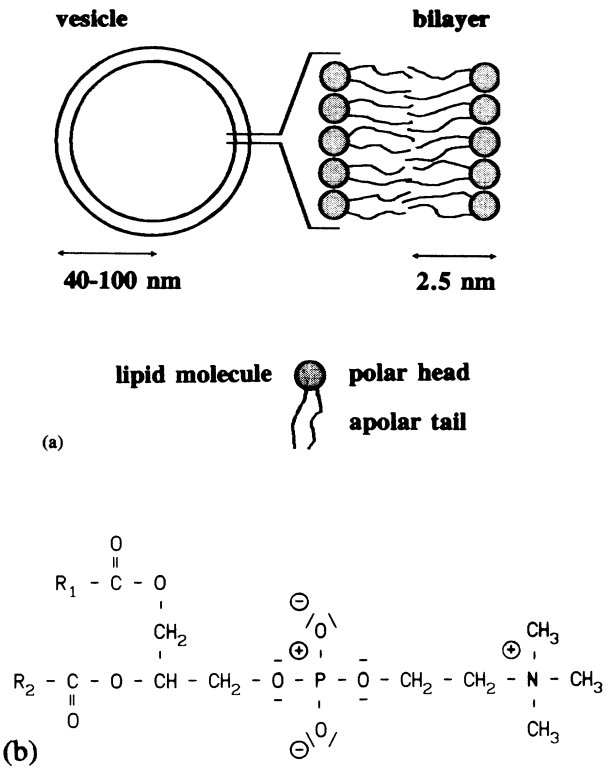

FIG. 2. (a) Structure of a vesicle and bilayer; (b) structure formula of the phosphatidyl choline molecule.

B. Preparation

The lipid vesicles of the present study were prepared according to the detergent removal recipe of Zumbuehl and Weder.[36] The vesicles consisted of a mixture of lipids: mainly unsaturated lipids extracted from egg yolk (EYL vesicles) (egg yolk lipids purchased from Lipid Products Ltd., United Kingdom). Bilayers of these lipids display a transition temperature trajectory and are in the fluid crystalline state from about 5 °C. The lipids have hydrophobic tails that contain 16, 18, or 20 carbon atoms. The unsaturated lipids can have one to four unsaturated bonds per aliphatic chain. Due to the unsaturated bonds in EYL lipids, they degrade quite rapidly. Care must therefore be taken to prevent long-time exposure of EYL vesicles to raised temperatures and oxygen.

Phosphatidyl choline lipids, which are used in this study, have no net charge. To prevent coagulation of the vesicles, a charge carrier in a mole fraction of 10% was included in the vesicle surface. The carrier used here is the *tris* salt of cholesteryl hemisuccinate (purchased from Sigma Chemical Company) and is negatively charged in the used buffer.

In the detergent-removal process, so-called mixed micelles are formed that consist of the material that is to be included in the vesicles bilayer and a detergent. Most detergents are molecules that have a polar head group and one more or less hydrophobic tail. It is important that they can associate with lipids as well as with water, making them very useful as solubilizing agents for lipids. Unlike lipids they are usually soluble in water. The nature of the detergent can have a significant influence on the vesicle formation: Factors affecting this formation are the critical micellar concentration (CMC), the presence of charge on the detergent head group, and the so-called hydrophile-lipophile balance (HLB) of the detergent.

After dissolving lipid and charge carrier together with the detergent [sodium cholate (purchased from Merck, Federal Republic of Germany)] in a chloroform-methanol mixture, the organic solvent is evaporated and on the inside of a round-bottomed flask a film is formed that is dried thoroughly. This film is dissolved in a buffer and a clear solution of small bilayer platelets (mixed micelles) is formed. The buffer that is used in this study is an isotonic phosphate buffer of pH 7.4 and an osmolarity of about 0.26. After the formation of mixed micelles, the solution is injected in cells that can each contain about 6 ml and that are separated from the dialysate by a membrane with a molecular weight cutoff of 5000 (Diachema, manufactured by Dianorm, Federal Republic of Germany). Eleven cells can be inserted in a device that slowly rotates in a glass tube which contains buffer that is continuously refreshed. In a thermostatted bath two such tubes can be placed, so that in each preparation cycle 132 ml of vesicle dispersion can be prepared. Dialysate volume is 1000 times the volume of the mixed micellar solution and dur-

ing 24 h the detergent is extracted from the micelles. During this process, the mixed micelles associate and, eventually, in a first-order process, form closed structures (vesicles). In a subsequent second-order process, excess detergent in the bilayer of the formed vesicles is washed away.

The whole prepration procedure is carried out at room temperature, which is well above the transition temperature, as it should be. After the preparation procedure, the vesicles are stored in a nitrogen atmosphere and a cool place ($T \simeq 4$ °C).

In the present study it will prove to be of vital importance to change the radius of the vesicles. An adaptation of the basic detergent-removal technique has been published by Schwendener *et al.*[37] where mixtures of different length alkyl glucopyramosides were chosen as detergent to form vesicles with radii to anywhere between 40 and 100 nm. In the present case different ratios of *n*-heptyl β-D glucopyranoside and *n*-octyl β-D glucopyranoside were applied (purchased from Serva, Federal Republic of Germany). For the larger radii the recipe is slightly altered in that a film is formed of only the lipid and charge carrier and that the detergent is added to this with the buffer. See Table I for an outline of the preparation conditions. It should be noted that the alkyl glucopyranosides dialyze much more rapidly than the sodium cholate. According to Weder and Zumbühl,[38] only when we are dealing with sodium cholate as detergent, may we expect some of it to still be present in the bilayer after 24 h of dialysis.

The preparation that we carried out yielded vesicles in a volume fraction of 3% to 8%, depending on the vesicle radius. For viscoelastic measurements the vesicle dispersion should be concentrated. Volume fractions of at least 25% are necessary. Concentration takes place in an Amicon Ultra Filtration device in which the buffer is forced through very small holes (radii ca. 10 nm) in a membrane, leaving the vesicles in a more concentrated state. As this takes quite a while (up to two days), the device is pressurized with nitrogen, and cooled to about 10 °C to prevent deterioration of the vesicles during concentration.

The preparation technique described here offers one of the most reliable routes to concentrated dispersions of unilamellar, monodisperse lipid vesicles, properties that are very important in the present study.

C. Characterization

The radius of the vesicles was obtained from dynamic light-scattering experiments. A sample of vesicles diluted with buffer to a volume fraction of about 0.5% was put in a laser beam and the 90° light scattering detected with a photomultiplier. The signal is Fourier transformed and in a curve fit the Fourier transform (FT) analyzed. The frequency where the FT height is halved is characteristic for the diffusion time of the vesicles. Together with known temperature, buffer viscosity, index of refraction of the buffer, and laser wavelength, we can then calculate the radius of the, supposedly, monodisperse vesicles. The error in this determination is typically 10% for vesicles of 40 to 100 nm radius.[39]

A direct way of accurately establishing the volume fraction ϕ of a vesicle dispersion is not trivial. The volume fraction can be estimated with a dry-weight method. With this method, ϕ is calculable if we know the lipid density in the bilayer, the bilayer thickness, and the vesicle radius. The uncertainties in these quantities, however, lead to an estimation of ϕ with large error margins. Here, we will determine ϕ by means of a measurement of the steady-state viscosity η_0' and a relationship between η_0' and ϕ that is known to exist from the literature. Formally, we hypothesize that vesicles behave as hard spheres under steady shear at low rates of shear and use the experimental relationship between η_0' and ϕ for hard spheres (Van der Werff and De Kruif[4]) to determine ϕ. Subsequently, this information is used in the analysis of the linear viscoelasticity measurements from which we conclude (Sec. V B) that the hard-sphere hypothesis correctly explains the experimental data.

IV. VISCOELASTIC MEASURING APPARATUS

For the study of the viscoelastic behavior in the frequency range of 70 Hz to 235 kHz, we have available two different types of apparatus, viz., the torsion pendulum and the nickel tube resonator. They have been described by Blom and Mellema[40] and Oosterbroek *et al.*,[41] respectively. Basically, with these instruments a harmonically oscillating shear is imposed on the dispersion. One term in the equation of motion is expressed in terms of the complex fluid impedance. Consequently, frequency and half-width of the resonance peak are influenced by the

TABLE I. Preparation conditions for the five vesicle samples. In the first column an identification number of the vesicle dispersion is given. In the second column, the preparation method is indicated. *A*, the film contains lipids and detergent, and buffer is added to it. *B*, the film contains only lipids and the detergent is added to it with the buffer. *L* is the lipid concentration, *L*:*D* is the molar lipid to detergent ratio for the following detergents: I, sodium cholate; II, *n*-octyl β-D glucopyranoside; III, *n*-heptyl β-D glucopyranoside. *a* is the vesicle hydrodynamic radius.

No.	Method	*L* (mmol/ml)	*L*:*D* I	II	III	*a* (nm)
1	*A*	0.013	0.5			36
2	*B*	0.013		0.6	0.2	60
3	*B*	0.013		0.53	0.24	65
4	*B*	0.013		0.4	0.35	70
5	*B*	0.013		0.25		106

properties of the fluid. For the determination of the steady-state shear viscosity a Contraves Low Shear viscometer was used.

A. The torsion pendulum

This pendulum is a cylindrical mass suspended from a heavy base plate by a torsion rod. The rod is made of a special material, called Thermelast, of which the temperature dependency of the torsion constant is strongly reduced. To the inside of the cylindrical mass is glued a magnet so that external excitation coils can induce a rotation. The pendulum rod will perform a torsion motion. The pendulum resonates with a characteristic frequency and half-width which will change according to the nature of the fluid in which it is immersed. The fluid impedance becomes part of the equation of motion.

In Fig. 3 a schematic drawing is presented of this measuring device. The base plate should be heavy so that its moment of inertia is large with respect to that of the cylindrical mass in view of suppressing the influence of external vibrations. The container in which the sample can be injected is thermostatted, as is the whole base plate, to prevent any major temperature leak. As the cylinder performs its oscillations, a second set of coils monitors the motion.

Basically, two measurements are required to determine the viscoelastic properties of a dispersion at a certain frequency. First, a measurement in air is performed, after which a measurement in the sample shows to which extent the position and half-width of the resonance peak have changed. The desired values of the viscous and elastic parts of the complex viscosity can then be determined.

The measurement of resonance peaks is largely computerized in that the computer first roughly searches for the position and half-width of the resonance peak and, after that, accurately scans the peak. Computation of the complex viscosity is done as well by the computer. The four torsion resonators that are used in this study oscillate with frequencies of about 70, 280, 690, and 2340 Hz. The amount of sample needed is about 20 ml for the first, 15 ml for the second, and 5 ml for the third and fourth resonators, respectively.

B. The nickel tube resonator

The nickel tube resonator is a hollow tube, 40 cm long, that is vertically suspended in a sealed glass tube, which is immersed in a thermostatted bath. See Fig. 4. The sample, about 15 ml, can be injected into the glass tube after which it completely surrounds the nickel tube.

Nickel is a magnetostrictive material. This means that the length of it increases along the magnetization direction as it is magnetized. The nickel tube that is used here has a permanent magnetization in the tangential direction along the tube wall. Placed coaxially along the symmetry axis of the tube is an excitation coil that, according to the applied frequency, superimposes an oscillating magnetization in the tube wall which is directed along the length of the tube. Together, these magnetizations result in a spirally oriented magnetization which is periodically directed towards the top and bottom of the tube. As the nickel tube elongates in the direction of the magnetization, the tube is forced on a torsional motion with the frequency of the signal in the excitation coil. However, due to boundary conditions, not all frequencies that are imposed will result in proper resonance waves that fit along the tube. There is, e.g., the condition that the tube, which is suspended on threads that hold the tube at length $\frac{1}{6}$ and $\frac{5}{6}$, has motional nodes there, as any actual movement at those sites will result in distorted motion. Furthermore, as the ends of the tube are unconnected, motional antinodes appear there and, lastly, as the excitation coil is situated at the center of the tube, a motional node should appear there, because motional modes mean maximum torsion and therefore most effective excitation. The registration coil is situated at $\frac{1}{6}$ or $\frac{5}{6}$ of the length of the tube. This is an ideal place for it since the restriction of a motional node appearing there happily means maximum torsion at that site, and, therefore, a measuring optimum. The result of the boundary conditions is that the tube will display a number of excited torsional modes that start with a frequency that corresponds to $4\frac{1}{2}$ wavelengths fitting along the length of the tube. From there on, every frequency that corresponds

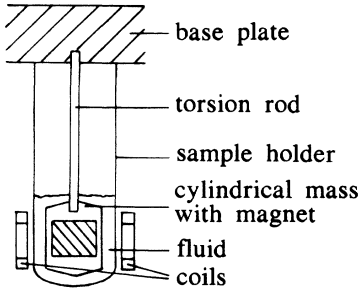

FIG. 3. Torsion pendulum.

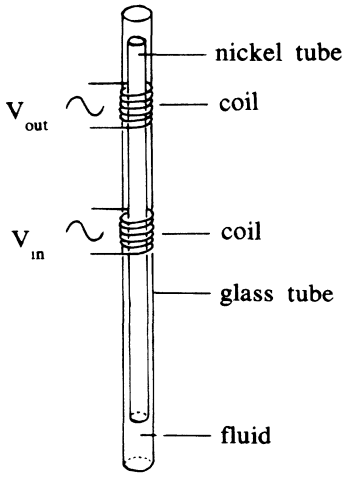

FIG. 4. Nickel tube resonator.

to $(4+3n)+\frac{1}{2}$ wavelengths along the tube is effectively excited. With one instrument, in this way, the fluid can be harmonically sheared with frequencies ranging from 4 to 235 kHz. From the possible feasible frequencies, in total 12 frequencies are, as a rule, used.

Unlike the material of which the torsion pendula are made, the frequency dependency of nickel on temperature is quite large. It is therefore important to have the apparatus thoroughly thermostatted. The temperature coefficient $\delta f/(f\delta T)$ of nickel is $17\times10^{-5}\,°C^{-1}$ (f is the frequency, T the temperature). Therefore, in order to obtain the frequency with an accuracy of better than 0.0002% (which is necessary for complex viscosities to be calculated with an accuracy of 1%), the temperature should remain constant to within 0.01 °C. This is easily attainable.

Measurement and calculation are computerized. As is the case with the torsion resonator, the computer searches roughly for the position and half-width of each of the 12 resonance peaks, and, after that, scans the peaks more accurately. For each frequency the viscous and elastic parts of the complex viscosity are calculated.

V. MEASUREMENTS AND RESULTS

A. Analysis

Linear viscoelastic measurements were carried out over the entire frequency range of 70 Hz to 235 kHz and at a temperature of 10.0 °C. The measurements show that for dispersions of lipid vesicles in water, two relaxation processes take place: The viscous part of the complex viscosity $\eta^*(\omega)$ decreases in two steps. See the figures of η^* that are presented in this paper: Figs. 5(a)–5(c).

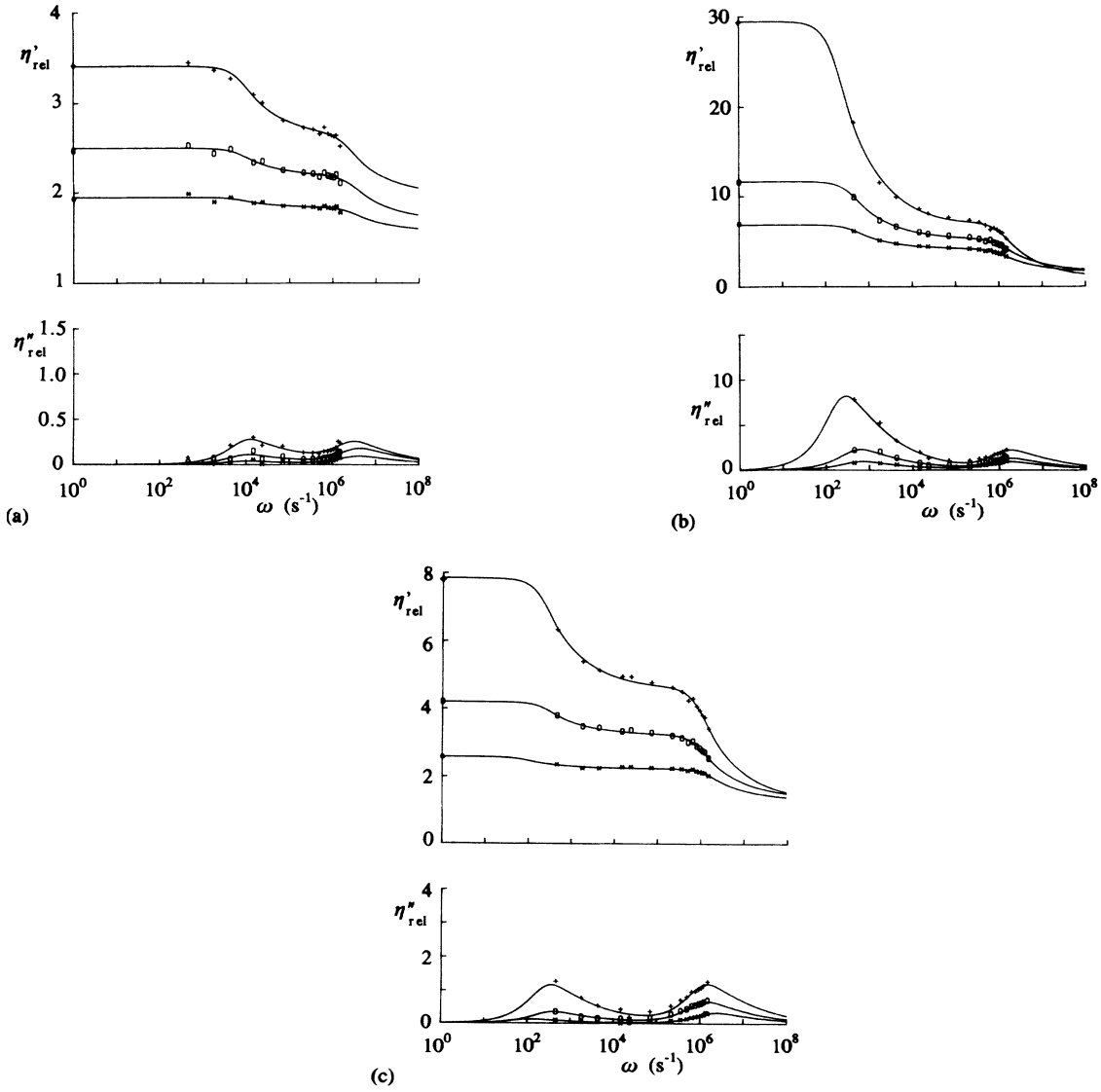

FIG. 5. (a) The relative complex viscosity $\eta^*/\eta_0=(\eta'-i\eta'')/\eta_0$ with $\eta_0=1.35$ mPa s of the 36-nm radius vesicles for $\phi=31\%$, 27%, and 24%. (b) The relative complex vicosity $\eta^*/\eta_0=(\eta'-i\eta'')/\eta_0$ with $\eta_0=1.35$ mPa s of the 70-nm radius vesicles for $\phi=51\%$, 44%, and 39%. (c) The relative complex viscosity $\eta^*/\eta_0=(\eta'-i\eta'')/\eta_0$ with $\eta_0=1.35$ mPa s of the 106-nm radius vesicles for $\phi=41\%$, 33%, and 28%.

The measurements of η' and η'' by themselves give a rough picture of the rheology of the fluid during oscillatory shear. In order to be able to deduce quantities from the viscoelastic measurements pertaining to microstructural properties as mentioned in Sec. II, the complex viscosity has to be analyzed. As will be found, the first relaxation process pertains to the self-diffusion of the vesicles in the dispersion. As has been proved experimentally by Van der Werff *et al.*,[3] this process of entropic relaxation is characterized by a series of relaxation times [Eq. (4)] rather than by a single time. It is found that the second relaxation process pertains to the viscoelasticity that characterizes the lipid bilayer of the vesicles. There is no reason to assume that only one deformation relaxation time process is involved, so for the second transition in η^* as a function of frequency a set of related times is also taken into account. Thus, phenomenologically, the governing equation for the real and imaginary parts of the observed complex viscosity are

$$\eta'(\omega)=\eta'_\infty+\sum_{i=1}^{M}\frac{G_{1,i}\tau_{1,i}}{1+\omega^2\tau_{1,i}^2}+\sum_{j=1}^{N}\frac{G_{2,j}\tau_{2,j}}{1+\omega^2\tau_{2,j}^2} \tag{14a}$$

and

$$\eta''(\omega)=\sum_{i=1}^{M}\frac{\omega G_{1,i}\tau_{1,i}^2}{1+\omega^2\tau_{1,i}^2}+\sum_{j=1}^{N}\frac{\omega G_{2,j}\tau_{2,j}^2}{1+\omega^2\tau_{2,j}^2}\ . \tag{14b}$$

It has been demonstrated experimentally by Van der Werff *et al.*[3] that for diffusion relaxation

$$\tau_{1,i}=\tau_{1,1}i^{-2}\equiv\tau_1 i^{-2}$$

and $G_{1,i}=G_{1,1}\equiv G_1$. Such a relationship is not known to exist for the deformation relaxation. In addition, there is the difficulty that the relevant observed transition in η^* could only be measured partially. Therefore, the analysis allows only an estimation of the longest relaxation time and the limit η'_∞. The estimation is systematized by assuming that the contribution of the shorter time processes with respect to the largest one is the same as in the diffusion case:

$$\tau_{2,j}=\tau_{2,1}j^{-2}\equiv\tau_2 j^{-2}$$

and $G_{2,j}=G_{2,1}\equiv G_2$. This may introduce a systematic error. This problem will be considered in the discussion. Thus five parameters determine the fit to η^*: η'_∞, τ_1, G_1, τ_2, and G_2. The fitting of the parameters of Eq. (14) to the data is carried out in a simultaneous fit to η' and η'' in order to get full advantage of the fact that information in the η' data adds to information in the η'' and vice versa.

As we now have the explicit expression that $\eta'(\omega)$ and $\eta''(\omega)$ must obey, the viscoelastic measurements on lipid vesicle dispersions can be fitted and the relevant data extracted. We have fitted the complex viscosity, including 100 times for both the first and second transition. In Tables II and III for a number of vesicle dispersions a survey is given of the fitted relaxation times and strengths for the various processes as well as some relevant expressions, among which are the scaled relaxation times and strengths. One may notice that

$$\eta'_0=\eta'_\infty+\sum_i G_{1,i}\tau_{1,i}+\sum_j G_{2,j}\tau_{2,j} \tag{15a}$$

and

$$\eta'_{\rm pl}=\eta'_\infty+\sum_j G_{2,j}\tau_{2,j}\ , \tag{15b}$$

where $\eta'_{\rm pl}$ represents the plateau value of $\eta'(\omega)$ between η'_0 and η'_∞.

B. The first relaxation process

Looking at Table II, one of the most prominent properties of the relaxation spectra is the way in which the position of the first peak shifts with varying vesicle radius. In Table II we have used the radius that was determined by dynamic light scattering. The first relaxation time and strength are functions of the third power of the radius.

TABLE II. Characteristics for the first relaxation process. In the first column an identification number of the vesicle sample is given. a is the hydrodynamic radius, ϕ is the volume fraction, η'_0 is the stationary viscosity, $\eta'_{\rm pl}$ is the plateau viscosity, $\eta'_{\rm eff,1}=\eta'_{\rm pl}+\frac{2}{3}(\eta'_0-\eta'_{\rm pl})$, and η_0 is the buffer viscosity at 10 °C: 1.35 mPa s.

No.	a (nm)	ϕ (%)	η'_0/η_0	$\eta'_{\rm pl}/\eta_0$	$\eta'_{\rm eff,1}$ (mPa s)	τ_1 (s)	G_1 (Pa)	$kT\tau_1/6\pi\eta_0 a^3$	$a^3G_1/kT\phi^2$	G_1/nkT
1a	36	31	3.41	2.63	4.26	$9.5\pm1.1\times10^{-5}$	6.9 ± 0.8	0.31 ± 0.10	0.86 ± 0.33	1.11 ± 0.38
1b	36	27	2.50	2.17	3.24	$1.0\pm0.2\times10^{-4}$	2.6 ± 0.6	0.33 ± 0.12	0.43 ± 0.18	0.49 ± 0.19
1c	36	24	1.96	1.83	2.59	$1.1\pm0.4\times10^{-4}$	$8.8\pm3.4\times10^{-1}$	0.36 ± 0.17	0.18 ± 0.09	0.18 ± 0.09
2	60	34	4.39	3.10	3.12	$5.7\pm0.6\times10^{-4}$	1.9 ± 0.2	0.41 ± 0.13	0.89 ± 0.33	1.27 ± 0.42
3	65	32	3.76	2.87	4.68	$7.5\pm0.8\times10^{-4}$	1.0 ± 0.1	0.42 ± 0.13	0.69 ± 0.26	0.92 ± 0.30
4a	70	51	29.4	6.76	29.5	$4.1\pm0.3\times10^{-3}$	4.6 ± 0.2	1.83 ± 0.57	1.56 ± 0.56	3.33 ± 1.07
4b	70	44	11.7	5.17	12.9	$1.9\pm0.1\times10^{-3}$	2.9 ± 0.2	0.83 ± 0.25	1.31 ± 0.47	2.41 ± 0.77
4c	70	39	6.82	4.12	8.01	$1.7\pm0.1\times10^{-3}$	1.3 ± 0.1	0.75 ± 0.23	0.77 ± 0.28	1.26 ± 0.40
5a	106	41	7.83	4.62	9.14	$3.3\pm0.3\times10^{-3}$	$8.1\pm0.7\times10^{-1}$	0.43 ± 0.14	1.47 ± 0.54	2.53 ± 0.81
5b	106	33	4.20	3.24	5.24	$2.9\pm0.4\times10^{-3}$	$2.7\pm0.3\times10^{-1}$	0.38 ± 0.12	0.77 ± 0.29	1.06 ± 0.35
5c	106	28	2.58	2.24	3.33	$9.9\pm2.8\times10^{-3}$	$2.8\pm0.8\times10^{-2}$	1.28 ± 0.53	0.11 ± 0.05	0.13 ± 0.05

TABLE III. Characteristics for the second relaxation process. In the first column, an identification number of the vesicle sample is given. a is the hydrodynamic radius, ϕ is the volume fraction, η'_{pl} is the plateau viscosity, η'_∞ is the infinite frequency viscosity level, $\eta'_{eff,2}=\eta'_\infty+\frac{2}{3}(\eta'_{pl}-\eta'_\infty)$, I equals $(23\eta_i+32\eta_{eff})(a-\frac{1}{2}h)$ (h is the bilayer thickness), and η_0 is the buffer viscosity at 10°C: 1.35 mPas.

	a (nm)	ϕ (%)	$\frac{\eta'_{pl}}{\eta_0}$	$\frac{\eta'_\infty}{\eta_0}$	$\eta'_{eff,2}$ (mPa s)	I (10^{-9} Pa s m)	τ_2 (10^{-7} s)	G_2 (kPa)
1a	36	31	2.63	2.0±0.2	3.2±0.7	4.51±0.7	2.75±1.00	1.97±1.27
1b	36	27	2.17	1.7±0.3	2.7±0.7	3.95±0.8	2.18±1.29	1.81±2.08
1c	36	24	1.83	1.6±0.2	2.3±0.4	3.56±0.5	2.18±1.47	1.00±1.24
2	60	34	3.10	1.8±0.1	3.6±0.4	8.41±1.0	4.69±0.61	2.26±0.49
3	65	32	2.87	1.8±0.1	3.4±0.2	8.76±1.0	4.29±0.39	1.98±0.27
4a	70	51	6.76	0.3±0.6	6.2±2.7	15.6±6.9	4.54±0.50	11.6±2.14
4b	70	44	5.17	1.6±0.2	5.4±1.0	13.7±2.1	5.20±0.40	5.71±0.70
4c	70	39	4.12	1.5±0.1	4.4±0.4	11.6±1.4	4.68±0.25	4.54±0.37
5a	106	41	4.62	1.3±0.1	4.7±0.5	18.9±2.4	6.88±0.36	3.87±0.30
5b	106	33	3.24	1.4±0.1	3.5±0.2	14.9±1.6	4.93±0.22	3.09±0.21
5c	106	28	2.24	1.3±0.1	2.6±0.2	11.9±1.3	4.12±0.37	1.85±0.29

This is predicted for diffusion relaxation. This dependency is illustrated by plots of $\eta^*(\omega)$ for vesicles with different radii at about the same volume fraction (Fig. 6).

Next, the influence of the volume fraction is considered. In Figs. 5(a), 5(b), and 5(c), we see plots of $\eta^*(\omega)$ of dispersions of vesicles of radius 36, 70, and 106 nm, each for three volume fractions. Note that the relaxation strength decreases unproportionally with the volume fraction: for 70 nm, as ϕ decreases 51%–44%–39%, the corresponding G_1 decreases 4.6–2.9–1.3 Pa. The vesicles of 106 nm show that for further reduction of the volume fraction, the first relaxation transition decreases in height even more completely out of proportion with the decrease of volume fraction: As ϕ decreases 41%–33%–28%, G decreases 0.8–0.3–0.03 Pa. From these figures it can safely be suggested that no process involving individual vesicles can be responsible, but that the process pertains to the interactions between the vesicles. This disproportionate effect of ϕ on relaxation strength has been predicted by theories on diffusion relaxation (Batchelor,[7] Russel and Gast,[8] and Wagner and Russel[9]) and supported by experiment (Van der Werff *et al.*[3]). The effect has been described by the increasing hindrance the diffusing particles experience from each other. Thus we now have two clues as to the nature of the first relaxation process. Some others can be given as well.

The relative viscosity of a dispersion of hard spheres in the limit of zero shear rate and zero frequency determined by Brownian motion and hydrodynamic interactions as a function of the volume fraction was measured by Van der Werff *et al.*[3] and theoretically approached by Batchelor,[7] Russel and Gast,[8] Wagner and Russel,[9] and semiempirically by Mooney[42] and Krieger and Dougherty.[34] At high frequencies another relative viscosity level of hard spheres is measured, determined by hydrodynamic interactions. The value of this level was predicted very well up to 45% by the theory of Beenakker.[43] The high-frequency relative viscosities of vesicle dispersions, which are here the viscosities after the first relaxation (the plateau viscosity, η'_{pl}), agree well with the experimentally determined viscosities given by Van der Werff *et al.*[3,44] (see Fig. 7). The line drawn in Fig. 7 is the fitted Krieger and Dougherty relation[34] with $[\eta]=2.5$ [Eq. (13)].

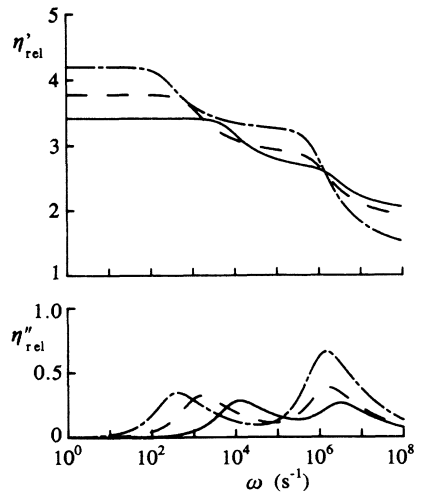

FIG. 6. The relative complex viscosity $\eta^*/\eta_0=(\eta'-i\eta'')/\eta_0$ with $\eta_0=1.35$ mPa s of three vesicle dispersions ($\phi\cong0.32$): ——, 1a (36 nm); — — —, 3 (65 nm); ---, 5b (106 nm).

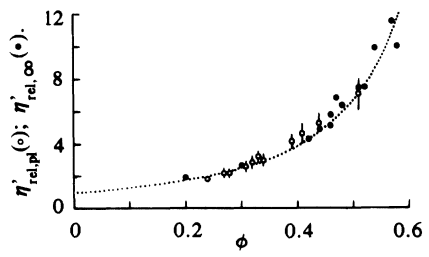

FIG. 7. Relative plateau viscosity (relative with respect to the solvent viscosity) for vesicles (○) and η'_∞ for silica particles (●) vs volume fraction. The dotted line is a fit according to the empirical expression by Krieger and Dougherty (Ref. 34) (with $[\eta]=2.5$), yielding $K_p=1.21$. Bars indicate typical errors.

In Figs. 8(a) and 9(a), the values of the expressions $kT\tau_1/6\pi\eta_0 a^3$ and $a^3G_1/kT\phi^2$, respectively, have been plotted for the measurements on various vesicle samples, together with the measurements on silica particles, reported by Van der Werff *et al.*[3,44] It can be seen that the scaled relaxation times and strengths of silica particles and vesicles corroborate each other.

As Fig. 8(a) suggests, the scaled relaxation times seem to be constant for low volume fractions, after which, around $\phi=0.5$, a sharp rise is observed. The $\phi=0$ limit for the expression, as derived by Batchelor [Eq. (2)], is 0.25. The present figure suggests this limit to be 0.35 ± 0.1: a first corroboration of theory by measurements. The sharp increase of $kT\tau_1/6\pi\eta_0 a^3$ for high volume fractions seems to be entirely due to the sharp increase in the effective viscosity experienced by a sphere during short-time self-diffusion, resulting in high relaxation times. The plot of $kT\tau_1/6\pi\eta_{\text{eff}}a^3$ versus ϕ [Fig. 8(b)] is therefore flat for high ϕ, as already noted by Van der Werff *et al.*[3] (the effective viscosity η'_{eff} a particle experiences during a transition in η^* can be stated as

$$\eta'_{\text{eff}}=\eta'\ (\omega\gg\tau^{-1})+\tfrac{2}{3}[\eta'(\omega\ll\tau^{-1})-\eta'(\omega\gg\tau^{-1})]$$

because this approximately is the viscosity η' at the largest relaxation time if the used series of relaxation times is taken into account).

The relaxation strength shows a clear increase for higher values of ϕ ($\phi>0.4$) [Fig. 9(a)]. The comparison of the present results with theory can only be done if the given G in theories is identified as G_1, wich has not yet been proved, but which is assumed here. The comparison is shown in a graph of G_1/nkT versus ϕ, in Fig. 9(b). It can be seen that the G_1 measurements of the vesicle and silica dispersions agree roughly with the predictions for G from Wagner and Russel[9] in case the superposition Percus-Yevick-type closure is used.

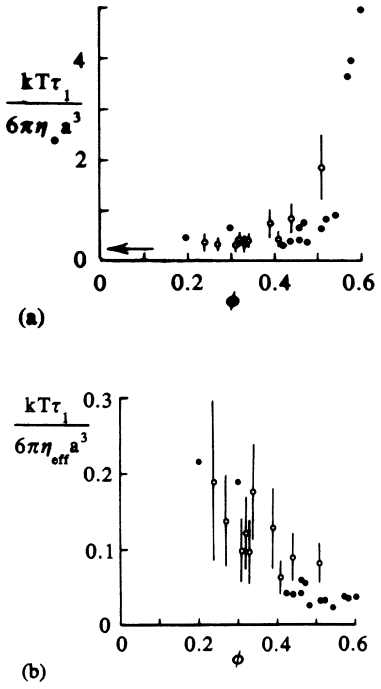

FIG. 8. (a) Scaled hard-sphere relaxation time $kT\tau_1/6\pi\eta_0 a^3$ vs volume fraction for dispersions of vesicles (○) and for silica particles (●). ← denotes the Batchelor limit. Bars indicate typical errors. (b) Scaled hard-sphere relaxation time $kT\tau_1/6\pi\eta_{\text{eff}}a^3$ vs volume fraction for dispersions of vesicles (○) and for hard spheres (●). Bars indicate typical errors.

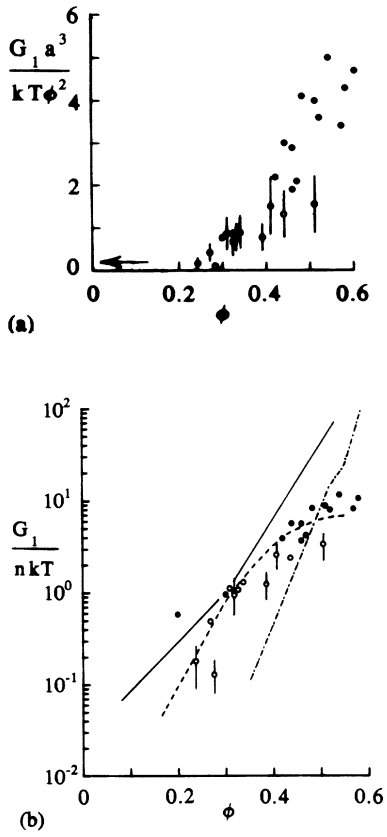

FIG. 9. (a) Scaled hard-sphere relaxation strength $a^3G_1/kT\phi^2$ vs volume fraction for dispersions of vesicles (○) and for silica particles (●). ← denotes the Batchelor limit. Bars indicate typical errors. (b) Scaled hard-sphere relaxation strength G/nkT, here assumed to be equal to G_1/nkT vs volume fraction for dispersions of vesicles (○) and for silica particles (●) with various theories included: ——, Russel and Gast; — — —, Wagner and Russel (superposition Percus-Yevick-type closure); —·—·—, Wagner and Russel (modified superposition). Some representative error bars are shown.

According to the theory of Batchelor,[7] $Ga^3/kT\phi^2$ [Fig. 9(a)] should have 0.21 as the $\phi\to0$ limit: The actual occurrence of this limit cannot be discarded. The weighed mean of the points below $\phi=0.3$, is namely,

$$G_1a^3/kT\phi^2\simeq0.25\pm0.1\ .$$

C. The second relaxation process

Viscoelastic measurements on vesicle dispersions also in principle provide relaxation times for a process pertaining to the deformation of the vesicles in shear flow. In Sec. II B it has been pointed out that the (elastic) con-

stants that are probably responsible for the observed relaxation process at the highest observable frequencies are γ, μ, and K_c.

The dependency of Eq. 9 on several parameters is complicated. In Table III it can be seen that the considered relaxation time τ_2 is approximately proportional to the radius at the same volume fraction ϕ and not much influenced by ϕ at the same radius. The former observation one would expect if $\gamma+\frac{2}{3}\mu$ is significantly larger than K_c/a_m^2. The latter observation one would expect if the relaxation of individual droplets is measured. In that case the influence of other droplets can be compensated for by replacing η_0 by η_{eff} in (9). Thus a plot of τ_2 versus $(23\eta_i+32\eta_{\text{eff}})a_m$, as is shown in Fig. 10, is appropriate to find other dependencies. No overall dependency on a_m^3 is seen, implying that $K_c/a_m^2 \ll (\gamma+\frac{2}{3}\mu)$. The influence of K_c is the strongest for small a_m values. Assuming the influence of K_c negligible for $(23\eta_i+32\eta_{\text{eff}})a_m$ larger than 6×10^{-9} Pa s m, a straight line through the τ_2 values of these points has a gradient $24(\gamma+\frac{2}{3}\mu)^{-1}$ and an ordinate cutoff of $16\zeta(\gamma+\frac{2}{3}\mu)^{-1}$. It follows that

$$\gamma+\tfrac{2}{3}\mu=(1.9\pm0.4)\times10^{-3}\text{N/m}$$

and

$$\zeta=(5.9\pm2.0)\times10^{-10}\text{ N s/m}\ .$$

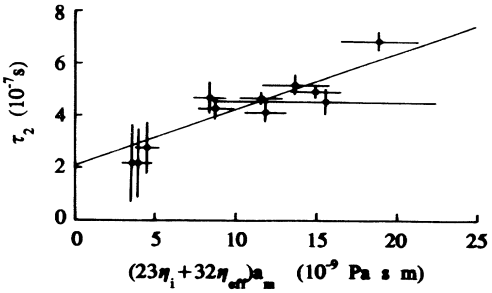

FIG. 10. Deformation relaxation time τ_2 vs $(23\eta_i+32\eta_{\text{eff}})a_m$ to determine $\gamma+\frac{2}{3}\mu$ and ζ.

With literature values of K_c in Table IV, it can be verified that the assumption turns out to be justified.

The two-dimensional microviscosity η_{mic} within the bilayer (the bilayer conceived as a two-dimensional continuum) can be obtained by dividing ζ by the membrane thickness (5 nm). Thus,

$$\eta_{\text{mic}}=120\pm40\text{ mPa s}\ .$$

We have established a value for the quantity $\gamma+\frac{2}{3}\mu$. We cannot specify how this quantiy is distributed among γ and μ. However, if we take a look at the literature (see Table IV), it can be seen that only very small values have

TABLE IV. Literature values of some bilayer mechanical constants for egg yolk lipid bilayers. Asterisk denotes upper limit; double asterisk is for varying lipid composition, including mixed unsaturated brain lipids.

Bilayer mechanical property	Literature values	Unit	Reference
Curvature modulus K_c	1–2	10^{-19} J	Schneider *et al.* (Refs. 24 and 25)
	0.4–0.5		Faucon *et al.* (Ref. 26)
	2.3±0.3		Servus *et al.* (Ref. 27)
	0.4		Engelhardt *et al.* (Ref. 28)
	1.1		Duwe *et al.* (Ref. 29)
	1.28±0.25		Bivas *et al.* (Ref. 30)
	0.5±0.5		Present work
	1.8±1.1		Present work and literature
Surface shear viscosity ζ	50–130*	10^{-10} N s/m	Waugh (Ref. 46)
	5.3		Wu *et al.* (Ref. 47)
	6		Wu *et al.* (Ref. 48)
	12		Wu *et al.* (Ref. 49)
	5.8±2.0		Present work
Microviscosity	180	mPa s	Bhattacharyya *et al.* (Ref. 50)
	120±40		Present work
Surface tension γ	$<10^{-2}$	10^{-3} N/m	Kwok and Evans (Ref. 31)
	$<10^{-5}$		Faucon *et al.* (Ref. 26)
Surface shear modulus μ	3.0±0.7	10^{-3} N/m	Present work
Dilatational modulus κ	140	10^{-3} N/m	Kwok and Evans (Ref. 31)
	70–150**		Mueller and Chien (Ref. 32)
	80±50		Present work and literature
Young's modulus E	2.3±0.5	10^6 Pa	Present work and literature
Poisson ratio ν	0.93±0.03		Present work and literature

been published for the interfacial tension of lipid bilayers [$\gamma \ll 10^{-3}$ N/m (Refs. 26 and 31)]. So, in the case of a negligible γ, we can give

$$\mu=(2.9\pm0.6)\times10^{-3}\ \text{N/m} .$$

From the deviations of the linear relationship of τ_2 versus $(23\eta_i+32\eta_{\text{eff}})a_m$ the value of K_c can be found using the deduced $\gamma+\frac{2}{3}\mu$ and ζ values. From Eq. (9) it follows that the quantity

$$Y=\frac{(23\eta_i+32\eta_{\text{eff}})a_m+16\zeta}{\tau_2}-16\mu \tag{16}$$

equals

$$24K_c(6-C_0a_m+\tfrac{1}{2}C_0^2a_m^2)/a_m^2 .$$

Two options for C_0 are interpretable. If the bilayer is composed of two identical layers, the spontaneous curvature C_0 equals 0. This is generally assumed. On the other hand, considering the preparation method it is not improbable that the layers are not identical but composed such that the spontaneous radius is identical to the produced radius, so C_0 equals $-2/a_m$. In Fig. 11, Eq. (16) is plotted versus $1/a_m^2$. When $C_0=-2/a_m$ [$a_0=a_m$ in Eq. (9)], it results in

$$K_c=(0.3\pm0.3)\times10^{-19}\ \text{J} .$$

The other case ($C_0=0$) gives

$$K_c=(0.5\pm0.5)\times10^{-19}\ \text{J} .$$

Apart from the relaxation time, the real part of the complex viscosity at low and high frequencies (with respect to τ_2^{-1}) can in principle also give information about a microstructural constant. Unfortunately, only intrinsic viscosities have been derived theoretically exactly. In Sec. V B η'_{pl} has been demonstrated to pertain to hard spheres with only hydrodynamic interactions. In the semitheoretical expressions for this plateau value (Krieger and Dougherty[34]), k_p is not known exactly, but is expected to be close to the inverse of the maximum volume fraction 0.74 but not necessarily equal to it. The measurements of η'_{pl} versus ϕ can be used to determine k_p

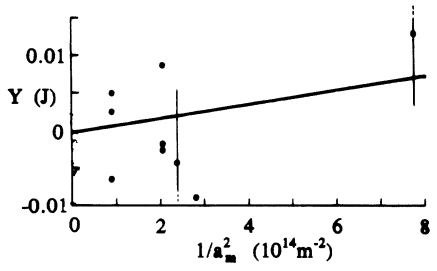

FIG. 11. Plot of $[(23\eta_i+32\eta_{\text{eff}})a_m+16\zeta]/\tau_2-16\mu$ ($=Y$) vs $1/a_m^2$ to determine K_c. Rightmost point is the average of the three Y values for the 36-nm vesicles. Left error is typical for the points with the exception of the right one.

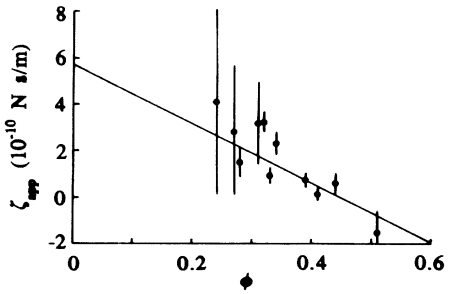

FIG. 12. Plot of $(a_m/16)(22[\eta'_\infty]_{\text{app}}\eta_0-7\eta_0)/(1-\frac{2}{5}[\eta'_\infty]_{\text{app}})$ vs ϕ to determine the volume-fraction dependency of ζ_{app}. This plot may be extrapolated to yield the actual ζ.

by fixing $[\eta'_{\text{pl}}]=\frac{5}{2}$. It follows that, fitting to Eq. (13),

$$k_p=1.21 ,$$

which is indeed different from $(0.74)^{-1}$. This fit of η'_{pl} versus ϕ, according to Eq. (13), can be found in Fig. 7, in which data for hard spheres are also included.

The limit η'_∞ is determined by spheres which are slightly ellipsoidally deformed. As pointed out in Sec. II B, k_p is for η'_∞ probably different from k_p for η'_{pl}. Consequently, by substituting k_p from η'_{pl} in the η'_∞ expression as given by Eq. (13), only an apparent intrinsic viscosity $[\eta'_\infty]_{\text{app}}$ is deduced which is still ϕ dependent. One can notice that $[\eta'_\infty]_{\text{app}}$ is dependent on a_m [Eq. (12)]. Substituting a deduced $[\eta'_\infty]_{\text{app}}$ in Eq. (12), using the relevant a_m value, an apparent ζ (ζ_{app}) can be deduced which is still dependent on ϕ:

$$\zeta_{\text{app}}=\frac{a_m}{16}\,\frac{\frac{2}{5}[\eta'_\infty]_{\text{app}}(55\eta_0)-7\eta_0}{1-\frac{2}{5}[\eta'_\infty]_{\text{app}}} . \tag{17}$$

If the used k_p from the hard-sphere viscosity accounts for the major part of the ϕ dependency of η'_∞, the dependency of ζ_{app} on ϕ may be so weak that an extrapolation of ζ_{app} to $\phi=0$ is possible to deduce ζ. In Fig. 12 ζ_{app} is shown as a function of ϕ. The ϕ dependency as found seems to be linear. Extrapolating to $\phi=0$, one finds

$$\zeta=(5.7\pm1.1)\times10^{-10}\ \text{N s/m} ,$$

which is in agreement with the ζ deduced from the τ_2 measurements. The uncertainty in this value is, apart from the statistical accuracy, related to the linear extrapolation. Because of the likeliness that the increase of ζ_{app} will weaken as the volume fraction decreases, this found ζ value might be too large, its lower boundary being about 4×10^{-10} N s/m. Its agreement with the ζ value from the τ_2 measurements, however, supports the linear extrapolation.

The relaxation strength of the second relaxation process is dependent on ϕ. No theories are available that calculate G_2 for fluctuating capsules in finite volume fractions. Neither can existing theories that calculate τ_2 and the viscosity levels η'_{pl} and η'_∞ for $\phi\to0$ (like Oldroyd's) be simply modified to account for any found G_2 for ϕ's in the measured volume-fraction range.

VI. DISCUSSION

In the complex viscosities as a function of frequency of dispersions of vesicles, two transitions can be discerned. The lowest frequency transition is convincingly interpreted as due to diffusion relaxation of hard spheres. The behavior of vesicles as hard spheres can easily be understood if an elastic constant, e.g., dilatational modulus or shear modulus, is assigned to the insoluble vesicle surface and the diffusion relaxation is slower than the deformation relaxation (Oldroyd[19,20] and Oosterbroek and Mellema[23]). The confrontation between theory and experiment raises questions which have been pointed out before (Van der Werff *et al.*[3]) but which have not yet been answered satisfactorily. The higher frequency transition pertains to deformation relaxation. An analysis problem is that it can only be partially measured. The first assumption that we used was based on the empirical fact that in rheology a single relaxation time process has never been observed alone. What is observed usually is the onset of one relaxation time process followed immediately by a set of other processes that possibly pertain to it. This leads to an asymmetric $\eta^*(\omega)$ transition like those drawn in Figs. 5(a)–5(c). A few factors can in principle cause an asymmetric transition here.

(1) The vesicle dispersions produced by the methods described in Sec. III are never 100% monodisperse. With light scattering we could demonstrate that the relative standard deviation is 10%–15%. Though this broadens the $\eta'(\omega)$ transition, even possibly asymmetrically, it seems improbable that this effect is significant since in the hard-sphere transition, a^3 plays a role and no clear deviation from the measurements done with the very monodisperse silica particles could be noticed.

(2) Another aspect is the possible excitations of higher deformation modes of the droplet surface. Higher deformation modes are calculated in several papers (Felderhof and Jones,[17] Van der Linden *et al.*,[18] Schneider *et al.*,[24] and Mellema *et al.*[45]). Two possibilities arise: (a) The deformation modes may be present due to thermal fluctuations around a spherical shape and sensed in oscillatory shear flow and (b) the vesicles may be deformed permanently at rest (thermal fluctuations zero) and forced to change shape in oscillatory shear flow. The former case has previously been considered for interfacial tension alone (Mellema *et al.*[45]). It turns out that, in case of elastic constants also, such higher modes are negligible in the present vesicle case. The argument reads as follows (see Mellema *et al.*[45]): The deformation energy of a mode is proportional to an elastic constant e (e.g., μ, κ, K_c/a_m^2, or a combination of them), to a_m^2, and the amplitude (the coefficient in the spherical harmonic series for the description of the shape) of the fluctuations squared. That energy is at thermal equilibrium proportional to kT (equipartition law). The relaxation strength for each mode is also proportional to ea_m^2 and the original amplitude squared with the exception of the lowest energy mode which is mainly proportional to ea_m^2 only. The largest contribution comes from the deformation of the equilibrium sphere (the lowest energy mode) being proportional to ea_m^2 while the higher modes are proportional to kT. Thus the individual relative contribution to the relaxation strength of a higher mode with respect to the lower is approximately kT/ea_m^2. Using the given constants $\mu=3\times10^{-3}$ N/m, $\kappa=0.1$ N/m, and $K/a_m^2\simeq10^{-5}$ N/m (for 100-nm vesicles, ea_m^2 then equals $7000kT$, 24×10^4 kT, and $24kT$, respectively), clearly higher modes are negligible. The case of permanent deformation cannot be excluded *a priori* but is very improbable because the always present thermal fluctuations allow the energy source to fade away any local presence of enhanced energy.

(3) Another possible cause which may lead to an asymmetric transition in η^* as a function of frequency is the $(1-i)\omega^{-1/2}$ dependency of η^* of the hard-sphere behavior at high frequencies (Van der Werff *et al.*[3]). If this dependency extends beyond frequencies at which the deformation relaxation occurs, (in Ref. 3, no indication of a limit was found), the observed deformation transition may be a single relaxation process on top of a $(1-i)\omega^{-1/2}$ background. Thus, to get still more insight into the consequences of our choice to systematize the procedure for the estimation of the longest relaxation time τ_2, an analysis has also been carried out with a single relaxation time for the deformation transition in two cases: (1) the hard-sphere tail $(1-i)\omega^{-1/2}$ is cut off before the onset of this time and (2) the tail is present as background. It follows that in case of the presence of the tail,

$$\mu=(3.2\pm0.6)\times10^{-3}\ \text{N/m}$$

and

$$\zeta=(6.3\pm2.0)\times10^{-10}\ \text{N s/m}\ ,$$

and in the absence of it,

$$\mu=(2.9\pm0.5)\times10^{-3}\ \text{N/m}$$

and

$$\zeta=(5.1\pm1.7)\times10^{-10}\ \text{N s/m}\ .$$

Clearly, these are similar results. They do not even differ significantly from

$$\mu=(2.9\pm0.6)\times10^{-3}\ \text{N/m}$$

and

$$\zeta=(5.9\pm2.0)\times10^{-10}\ \text{N s/m}\ ,$$

the result from the analysis where 100 deformation relaxation times have been taken into account (see Sec. V C). Surveying these analysis results, one may conclude that the possible systematic error due to the analysis procedure falls within the statistical error boundaries, unless more exotic influences of shorter time processes are present. Consequently, we propose as best values

$$\mu=(3.0\pm0.7)\times10^{-3}\ \text{N/m} \tag{18a}$$

and

$$\zeta=(5.8\pm2.0)\times10^{-10}\ \text{N s/m}\ . \tag{18b}$$

The values of η'_∞ in Table III have to be considered with suspicion, as η'_∞ is much more sensitive than τ_2 to

the choice of the number of times. However, as we have shown, the information to be drawn from η'_∞ is scarce. So, uncertainties in η'_∞ do not influence our conclusions.

Now we are able to find E and ν values using some literature data. From Table IV we conclude that for egg-yolk-lipid bilayers K_c varies between 0.4 and 2.6×10^{-19} J and κ varies between 0.07 and 0.15 N/m. In Fig. 13, $E(\nu)$ functions are plotted according to Eqs. 8(a), 8(b), and 8(c) using in each the μ, κ, or K_c boundary values from (18a) or literature data. Each $E(\nu)$ function plotted this way defines an area in which E and ν values are possible, given the boundary values of μ, κ, or K_c. The following E and ν values can now be deduced as these determine the region in the plot that is shared by all three $E(\nu)$ areas:

$$E=(2.3\pm0.5)\times10^6 \text{ Pa}$$

and

$$\nu=0.93\pm0.03 .$$

The Poisson ratio pertains to two-dimensional deformation. One may observe that the values for μ are vital in this case, as they rigorously restrict the common area of κ and K_c alone, which would extend from $\nu=0.12$ to $\nu=1$. The elastic constants corroborate each other when

$$\mu=(3.0\pm0.7)\times10^{-3} \text{ N/m} ,$$

$$\kappa=0.08\pm0.05 \text{ N/m} ,$$

and

$$K_c=(1.8\pm1.1)\times10^{-19} \text{ J} .$$

Apart from these elastic constants, the surface shear viscosity has been found. Its value, $(5.8\pm2.0)\times10^{-10}$ N s/m, agrees very well with literature values in Table IV. This agreement further justifies the analysis.

Another aspect has to be considered yet. The preparation of the vesicles requires detergent that should be removed completely. For different radii, different detergents are used which may not have been completely removed: in particular, sodium cholate (see Sec. III). Considering the results (Fig. 10), within the accuracy no indication is found for a possible difference in composition of the vesicle surface. Also the agreement of the deduced material constants with literature values from differently prepared EYL bilayers sustains this view.

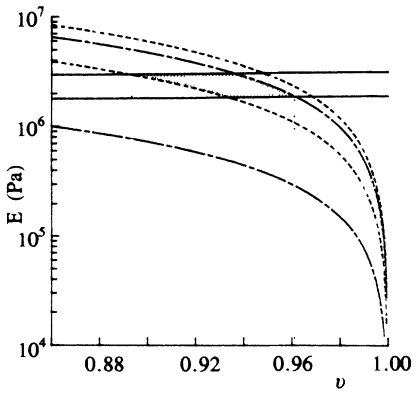

FIG. 13. Areas of $E(\nu)$ determined by boundaries of μ, κ, and K_c: ——, pertaining to μ; — — —, pertaining to κ; and — — —, pertaining to K_c. The hatched region is common.

VII. CONCLUSIONS

Summarizing, we conclude that vesicles show hard-sphere behavior in oscillating flow at lower frequencies, but are deformed at higher frequencies. Newly deduced is the surface shear modulus of EYL bilayers. The found surface shear viscosity is in agreement with literature values. The shear modulus provides the additional information to be able to extract from literature the Young's modulus and the surface Poisson ratio for EYL bilayers. Thus, also the surface dilatational modulus and curvature modulus consistent with the found surface shear modulus could be given. One may notice that this is the first time that with bulk rheological means surface rheological parameters are deduced. These parameters are established for such tiny particles that other methods are hard to imagine.

ACKNOWLEDGMENTS

The authors wish to thank Ir. F. K. Feenstra for his contribution during the initial stages of this research.

[1]A. K. Van Helden, J. W. Jansen, and A. Vrij, J. Colloid. Interface Sci. **81**, 354 (1981).
[2]S. Coehen and C. De Kruif, J. Colloid. Interface Sci. **124**, 104 (1988).
[3]J. C. Van der Werff, C. G. De Kruif, C. Blom, and J. Mellema, Phys. Rev. A **39**, 795 (1989).
[4]J. C. Van der Werff and C. G. De Kruif, J. Rheol. **33**, 421 (1989).
[5]H. Fröhlich and R. Sack, Proc. R. Soc. London, Ser. A **185**, 415 (1946).
[6]W. Flügge, in *Viscoelasticity* (Springer-Verlag, Berlin, 1975).
[7]G. K. J. Batchelor, J. Fluid Mech. **83**, 97 (1977).
[8]W. B. Russel and A. P. Gast, J. Chem. Phys. **84**, 1815 (1986).
[9]N. J. Wagner and W. B. Russel, Physica A **155**, 475 (1989).
[10]R. Aris, in *Vectors, Tensors and the Basic Equations of Fluid Mechanics* (Prentice-Hall, Englewood Cliffs, NJ, 1962).
[11]R. A. De Bruijn and J. Mellema, Rheol. Acta. **24**, 159 (1985).
[12]P. G. De Gennes and C. Taupin, J. Phys. Chem. **86**, 2294 (1982).
[13]W. Helfrich, Z. Naturforsch. Teil C **28**, 693 (1973).
[14]M. Kléman, Proc. R. Soc. London, Ser. A **347**, 387 (1976).
[15]P. Seide, in *Small Elastic Deformations of Thin Shells* (Noordhoff, Leiden, Holland).
[16]P. Brunn, Biorheology **17**, 419 (1980).

[17]B. U. Felderhof and R. B. Jones, Physicochemical Hydrodynamics **11**, 507 (1989).
[18]E. Van der Linden, D. Bedeaux, and M. Borkovec, Physica A **162**, 99 (1989).
[19]J. G. Oldroyd, Proc. R. Soc. London, Ser. A **218**, 122 (1953).
[20]J. G. Oldroyd, Proc. R. Soc. London, Ser. A **232**, 567 (1955).
[21]D. Barthes-Biesel and V. Chhim, Int. J. Multiphase Flow **7**, 493 (1981).
[22]Y. Takano and A. Sakanishi, Biorheology **21**, 405 (1984).
[23]M. Oosterbroek and J. Mellema, J. Colloid. Interface Sci. **84**, 14 (1981).
[24]M. B. Schneider, J. T. Jenkins, and W. W. Webb, J. Phys. (Paris) **45**, 1457 (1984).
[25]M. B. Schneider, J. T. Jenkins, and W. W. Webb, Biophys. J. **45**, 891 (1984).
[26]J. F. Faucon, M. D. Mitov, P. Méléard, I. Bivas, and P. Bothorel, J. Phys. (Paris) **50**, 2389 (1989).
[27]R. M. Servus, W. Harbich, and W. Helfrich, Biochim. Biophys. Acta **436**, 900 (1976).
[28]H. Engelhardt, H. P. Duwe, and E. Sackman, J. Phys. (Paris) Lett. **46**, L395 (1985).
[29]H. P. Duwe, H. Engelhardt, A. Zilker, and E. Sackmann, Mol. Cryst. Liq. Cryst. **152**, 1 (1987).
[30]I. Bivas, P. Hanusse, P. Bothorel, and J. Lalanne, and O. Aguerre-Chariol, J. Phys. (Paris) **48**, 855 (1987).
[31]R. Kwok and E. A. Evans, Biophys. J. **35**, 637 (1981).
[32]P. Mueller and T. F. Chien, Biophys. J. **44**, 375 (1983).
[33]S. T. Milner and S. A. Safran, Phys. Rev. A **36**, 4371 (1987).
[34]I. M. Krieger and T. J. Dougherty, Trans. Soc. Rheol. **3**, 137 (1959).
[35]R. C. Ball and P. Richmond, Phys. Chem. Liq. **9**, 99 (1980).
[36]O. Zumbuehl and H. G. Weder, Biochim. Biophys. Acta **640**, 252 (1981).
[37]R. A. Schwendener, M. Asanger, and H. G. Weder, Biochem. Biophys. Res. Commun. **100**, 1055 (1981).
[38]H. G. Weder and O. Zumbuehl, in *Liposome Technology,* edited by G. Gregoriadis (CRC, Boca Raton, FL, 1984).
[39]N. De Jaeger, R. Sneyers, H. Demeyere, J. Vanderdeelen, P. Van der Meeren, M. Van Laethem, and R. Finsy (unpublished).
[40]C. Blom and J. Mellema, Rheol. Acta **23**, 98 (1984).
[41]M. Oosterbroek, S. S. Wiseall, E. G. Altena, J. Mellema, and G. A. M. Kip, Rheol. Acta **19**, 497 (1980).
[42]M. Mooney, J. Colloid. Sci. **6**, 162 (1951).
[43]C. W. J. Beenakker, Physica A **128**, 48 (1984).
[44]J. C. Van der Werff and C. G. De Kruif, data for $\phi=0.2$ and $\phi=0.3$ (private communication).
[45]J. Mellema, C. Blom, and J. Beekwilder, Rheol. Acta **26**, 418 (1987).
[46]R. E. Waugh, Biophys. J. **38**, 29 (1982).
[47]E. Wu, K. Jacobson, and D. Papahadjopoulos, Biochemistry **16**, 3936 (1977).
[48]E. Wu, K. Jacobson, F. Szoka, and A. Portis, Biochemistry **17**, 5543 (1978).
[49]E. S. Wu, P. S. Low, and W. W. Webb, Biophys. J. (Abstr.) **33**, 109a (1981).
[50]M. Bhattacharyya, B. B. Bhowmik, and P. Nandy, Arch. Biochem. Biophys. **263**, 117 (1988).

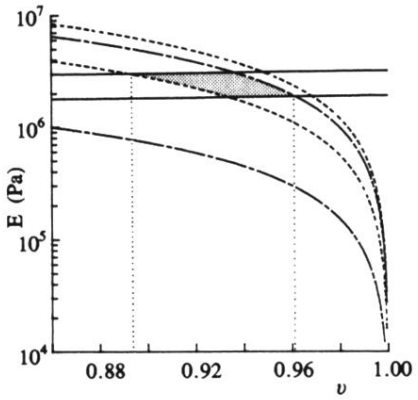

FIG. 13. Areas of $E(\nu)$ determined by boundaries of μ, κ, and K_c: ——, pertaining to μ; — — —, pertaining to κ; and —·—·-, pertaining to K_c. The hatched region is common.

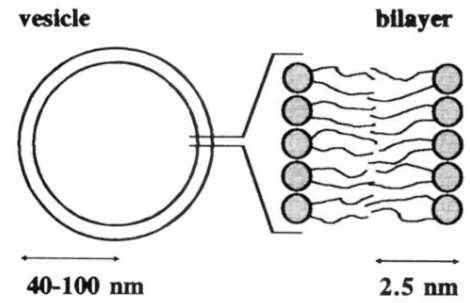

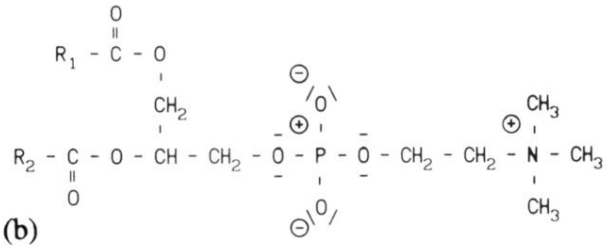

FIG. 2. (a) Structure of a vesicle and bilayer; (b) structure formula of the phosphatidyl choline molecule.